A 439-year simulated daily discharge dataset (1861-2299) for the upper Yangtze River, China

Chao Gao[1], Buda Su[2], Valentina Krysanova[3], Qianyu Zha[1], Cai Chen[1], Gang Luo[1], Xiaofan Zeng[4], Jinlong Huang[5], Ming Xiong[6], Liping Zhang[7], Tong Jiang[5]

5 [1]Department of Geography & Spatial Information Techniques, Ningbo University, Ningbo, 315211, China;
[2]National Climate Centre, China Meteorological Administration, Beijing 100081, China;
[3]Potsdam Institute for Climate Impact Research, Potsdam, Germany;
[4]School of Hydropower and Information Engineering, Huazhong University of Science and Technology, Wuhan, 430074, China;
10 [5]Collaborative Innovation Center on Forecast and Evaluation of Meteorological Disasters, Institute for Disaster Risk Management, School of Geographical Science, Nanjing University of Information Science & Technology, Nanjing 210044, China;
[6]Bureau of Hydrology, Changjiang River Water Resources Commission, Wuhan, 430010, China;
[7]State Key Laboratory of Water Resources and Hydropower Engineering Science, Wuhan University, Wuhan, 430072, China

15 *Correspondence to*: Tong Jiang (jiangtong@nuist.edu.cn)

Abstract The outputs of four Global Climate Models (GFDL-ESM2M, HadGEM2-ES, IPSL-CM5A-LR and MIROC5), which were statistically downscaled and bias corrected, were used to drive four hydrological models (HBV, SWAT, SWIM and VIC) to simulate the daily discharge at the Cuntan hydrological station in the upper Yangtze River from 1861 to 2299. As the performances of hydrological models in various climate conditions could be different, the models were first calibrated in the
20 period from 1979 to 1990. Then, the models were validated in the comparatively wet period, 1967 - 1978, and in the comparatively dry period, 1991 - 2002. A multi-objective automatic calibration programme using a univariate search technique was applied to find the optimal parameter set for each of the four hydrological models. The Nash-Sutcliffe efficiency (NSE) of daily discharge and the weighted least squares function (WLS) of extreme discharge events, represented by high flow (Q10) and low flow (Q90), were included in the objective functions of the parameterization process. In addition, the simulated
25 evapotranspiration results were compared with the GLEAM evapotranspiration data for the upper Yangtze River basin. For evaluating the performances of the hydrological models, the NSE, modified Kling-Gupta efficiency (KGE), ratio of the root mean square error to the standard deviation of the measured data (RSR) and Pearson's correlation coefficient (r) were used. The four hydrological models reach satisfactory simulation results both in the calibration and validation periods. In this study, the daily discharge is simulated for the upper Yangtze River under the preindustrial control (piControl) scenario without
30 anthropogenic climate change from 1861 - 2299, and for the historical period 1861 - 2005 and for 2006 to 2299 under RCP2.6, RCP4.5, RCP6.0 and RCP8.5 scenarios. The long-term daily discharge dataset can be used in the international context and water management, e.g. in the framework of Inter-Sectoral Impact Model Intercomparison Project (ISIMIP) by providing clue to what extent human-induced climate change could impact streamflow and streamflow trend in future. The datasets are available at the https://doi.org/10.4121/uuid:8658b22a-8f98-4043-9f8f-d77684d58cbc (Gao et al., 2019).

1 Introduction

Global warming is the long-term rise in average temperature of the earth's climate system. Warming temperature alters global water circulation processes and could significantly influence the sustainability of society and economy (Jung et al., 2011). The variation in water resource availability in the context of global warming is acknowledged as a focus of many international research projects (Stagl et al., 2016; Raman et al., 2018; Maisa et al., 2019). The long-term accurate (as much as possible) daily discharge time series are crucial for in-depth understanding of the changes in streamflow, and they are needed for subsequent climate change impact studies. However, discharge is monitored usually only for short observational periods in most river basins.

For generation of the long-term streamflow series, many data mining techniques including the sedimentological method, the hydrological field survey method, and the documentary analysis method can be applied (Longfield et al., 2018). Nevertheless, low temporal resolution and insufficient accuracy of these estimations can hardly meet the demands of practical and research applications. Instead, the observed climatic variables and the outputs of climate models have often been used to drive hydrological models to evaluate changes in streamflow in the context of climate change (Braud et al., 2010; Chen et al., 2017; Su et al., 2017; Dahl, 2018; Seneviratne et al., 2018). But there is lack of research on the quantitative estimation of long-term streamflow for period longer than 400 years under different scenarios with and without anthropogenic climate change (Meaurio, 2017).

The Yangtze River is the longest river in China. It originates from the Tibetan Plateau and enters the East China Sea after flowing through 11 provinces. With a large topographic gradient and substantial water supply of approximately 10,000 m^3s^{-1} on the average, the upper Yangtze River is rich in hydropower resources, but subjected to destructive flash floods. The Yangtze River has the longest hydrological observations in China. Data provided by the Cuntan hydrological station, which started operating in 1939, facilitates hydro-meteorological studies in the instrumental period (Su et al., 2008; Wang et al., 2008; Su et al., 2017). As changes in streamflow at the Cuntan station directly influence inflow to the Three Gorges Reservoir, establishing long-term discharge series at the Cuntan station can support effective management of hydraulic projects. Besides, the longer discharge series can also provide a possibility to explore impacts of anthropogenic climate change on hydrology for international climate change research community. Therefore, we simulated daily discharge at the Cuntan hydrological station in the upper Yangtze River in the period 1861 - 2299 using available climate model outputs.

The outputs of four downscaled GCMs (GFDL-ESM2M, HadGEM2-ES, IPSL-CM5A-LR, and MIROC5) are utilized to drive four hydrological models (HBV, SWAT, SWIM and VIC) to simulate discharge at the Cuntan station. The climate forcing comprise (a) the scenario with anthropogenic climate change for the period 1861 - 2299, which is subdivided into the historical period (1861 - 2005) and the future period (2006 - 2299) under different Representative Concentration Pathways (RCPs), and

(b) the preindustrial control scenario (piControl) for the period 1861 - 2299, which is used as a reference to detect the influence of anthropogenic climate change on streamflow in the upper Yangtze River.

2 Study Area

The catchment area of the Cuntan hydrological station (29 ° 37 ′ N, 106 ° 36 ′ E) in the upper Yangtze River is approximately 860,000 km^2, and 352.7 billion m^3 water is flowing through this point annually with average discharge of 109,34 m^{3}s^{-1} in the period of instrumental measurements beginning in 1939. Location of the Cuntan hydrological station, 311 GCM grids, meteorological stations and spatial distribution of the land use and soil types in the upper Yangtze River basin are shown in Fig. 1. Prairie grassland and acid purple soil are the most widespread of land use and soil type in the upper Yangtze River basin. The upper Yangtze River have complex geomorphic types and broken topography. Mountains and plateaus account for most of the region, hills and plains are few. Influenced by the East Asia subtropical monsoon and a complex topography, climate varies across the basin with annual air temperature and precipitation being high in the southeast but low in the northwest headstream region. According to observational data, the areal averaged annual mean temperature and precipitation are 12.3 ℃ and 1018 mm, respectively, during 1961 - 2017 in the upper Yangtze River basin.

3 Data and Methods

3.1 Climate scenarios

The outputs of the GCMs (GFDL-ESM2M, HadGEM2-ES, IPSL-CM5A-LR, and MIROC5) were statistically downscaled and bias corrected on a regular 0.5 × 0.5 ° resolution grid using a first-order conservative remapping scheme (Frieler et al., 2017; Lange, 2018). The GFDL model was developed by the Geophysical Fluid Dynamics Laboratory, Princeton University, USA, and all its integrations (approximately 100 in total), including GFDL-ESM2M and GFDL-ESM2G, were completed for the Coupled Model Intercomparison Project Phase 5 (CMIP5) protocol (Taylor et al., 2012). HadGEM2-ES is a coupled earth system model that was developed by the Met Office Hadley Centre, UK, for the CMIP5 centennial simulations (Jones et al., 2011). The IPSL-CM5A-LR model was developed by the Institute Pierre Simon Laplace, France, and the model was built around a physical core that includes atmosphere, land surface, ocean and sea ice components (Dufresne et al., 2013). MIROC5 is a new version of the atmosphere-ocean GCM that was developed by the Japanese research community (Watanabe et al., 2010).

Lack of long-term homogeneous observational data and existing of confounding influence from socioeconomic drivers, make GCM simulations rarely cover the preindustrial period. In this study, climate simulations include a piControl scenario, representing a climate with natural variability under stable CO_2 concentration of 286 ppm; a historical scenario, representing

the historical CO_2 concentration; and future RCP scenarios, representing various future CO_2 concentration pathways. The availability of climate scenarios for the different periods is shown in Table 1 (see also Frieler et al., 2017). Note that not all simulations cover 22nd and 23rd century. Data after 2099 are available from three models under RCP2.6, only from IPSL under RCP4.5 and RCP8.5, but no simulations under RCP6.0.

3.2 Observed meteorological and hydrological data

The observed daily meteorological data for 1951 - 2017 from 189 ground-based stations in the upper Yangtze River Basin used in this study were quality controlled by considering changes in instrument type, station relocations, and trace biases at the National Meteorological Information Centre of China Meteorological Administration (Ren et al., 2010), which was inputted into the hydrological models by spatial interpolation. During 1951 - 2017, annual precipitation shows a decreasing trend, with multi-year average of 935 mm, and annual mean temperature has shown a positive trend with multi-year average of 10.5 ℃. The daily discharge record at the Cuntan station in the upper Yangtze River is available for 1970 - 1999 from the China Hydrological Yearbook - Yangtze. The rest of daily record for periods 1939 - 1969 and 2000 - 2012 is collected from the Changjiang Water Resources Commission, Ministry of Water Resources in China.

The Yangtze River is prone to be flooded because of large inter- and inner-annual variations of precipitation. The most severe flood that can be tracked in the upper Yangtze River occurred in 1870, with a flood peak of approximately 100,500 m^3s^{-1} at the Yichang station located downstream of the Cuntan station (Changjiang Water Resources Commission, 2002). The peak flows reached 63,600 m^3s^{-1} and 64,600 m^3s^{-1}, respectively, at the Cuntan station and the Yichang station during the 1931 flood, and 52,200 m^3s^{-1} and 66,800 m^3s^{-1}, respectively, during the 1954 flood (Hu and Luo, 1992; Luo and Le, 1996). During the strongest flood of the 20th century in the Yangtze River, the peak flow at the Cuntan station reached 68,500 m^3s^{-1} in 1998 (Changjiang Water Resources Commission, 2002).

3.3 GLEAM evapotranspiration data

Evapotranspiration data from the Global Land Evaporation Amsterdam Model (GLEAM) for 1986 - 2005 that were released by the University of Bristol (Miralles et al., 2011) are used in our study to cross-check the performances of the hydrological models by means of the geographic information system (GIS) tools. The GLEAM data was generated based on a variety of satellite-sensor products at monthly scale with a spatial resolution of 0.25°. The spatial distributions of simulated evapotranspiration with that from GLEAM are compared by GIS techniques, and kappa value of confusion matrix is also applied to evaluate the accuracy of simulated evapotranspiration (taking VIC output as an example) by refer to GLEAM.

3.4 Hydrological models and parameterization

Four hydrological models, HBV (Bergstrom et al., 1973), SWAT (Arnold et al., 1998), SWIM (Krysanova et al., 2005) and

VIC (Liang et al., 1994) are used to simulate river discharge at the Cuntan hydrological station, and a flowchart of the hydrological modelling process is shown in Fig. 2. A brief introduction to these four hydrological models is given in Table 2 (see also Hattermann et al., 2017).

The univariate search technique, which can evaluate the informativeness of each feature individually, is used to calibrate the parameters. The objective functions include the Nash-Sutcliffe efficiency (NSE) of daily discharge (Nash and Sutcliffe, 1970) and the weighted least squares function (WLS) of high flow (Q10) and low flow (Q90). To achieve the maximum NSE and the minimum gap between the observed and the simulated, parameterization processes are iterated over 2,000 times within the ranges of the valid parameter scopes in Table 3 (Lai et al., 2006).

For evaluating daily hydrograph simulation, ratio of the root mean square error to the standard deviation of measured data (RSR) is recommended (Moriasi et al., 2007). In addition, the Kling-Gupta efficiency (KGE) was developed to provide diagnostic insights into the model performance by decomposing the NSE into three components: correlation, bias and variability (Gupta et al., 2009). In this study, four criteria, the NSE, RSR, Pearson's correlation coefficient (r) and KGE, are applied to the daily discharge series to evaluate the performance of hydrological models (Krysanova et al., 2018; Table 4) .Thresholds of acceptance of four criteria are derived from the references (Nash and Sutcliffe, 1970; Moriasi et al., 2007; Huang et al., 2012; King et al., 2012).

3.5 Geospatial information

A digital elevation model (DEM) with a resolution of 90 m from the Shuttle Radar Topography Mission database is used in this study. The soil property data is obtained from the Harmonized World Soil Database of the Food and Agriculture Organization of the United Nations (http://www.fao.org/), and the spatial distribution of soil types (1:1,000,000) is taken from the Institute of Soil Science, Chinese Academy of Sciences (CAS). A land use map of 1990 (1:1,000,000) from the Data Center for Resource and Environmental Sciences, CAS is applied for all hydrological runs under various climate conditions including the piControl, the historical and the RCP scenarios.

4 Results

4.1 Climate change in the upper Yangtze River basin

According to ensemble mean of four GCMs, annual mean temperature in the upper Yangtze River basin in the period 1986 - 2005 is 0.49 °C higher than that in the period 1861 - 1900, the increase is lower than the global average of 0.61 °C in the same period. Compared to the piControl scenario, annual mean temperature is projected to increase significantly in the 21st century, by 1.85 ~ 3.31 °C under RCPs. After 2100, surface air temperature will remain stable under RCP2.6 and increase only slightly under RCP4.5, but a significant increase in temperature will continue under RCP8.5, with an increase up to 13.5 °C by 2299

compared to the piControl scenario (Fig. 3a, Table 5). The visible abruption in temperature in the year 2100 under RCP4.5 and RCP8.5 in Fig. 3a are due to the fact that only the IPSL model runs are available after 2100 for these scenarios.

The long-term average monthly dynamics of temperature show a single-peak curve, with July is the hottest month. In the period 1861-2005, the inner-annual distribution pattern of temperature is very similar for the piControl and the historical scenarios (Fig. 3b). However, differences in the monthly temperatures between RCPs and piControl scenario become apparent with time (Fig. 3c-d). Taking the temperature in July as an example, difference between the two scenarios are approximately 1.9 ~ 3.2 °C in the 21st century but will enlarge to 1.7 ~ 12 °C in the period 2100 - 2299.

Compared with precipitation under piControl scenario, which has no monotonic trend, annual precipitation is approximately 2 % (16 mm) less in 1861 - 2005 under historical scenario. With relative to the piControl scenario, changes of annual precipitation will be -1.2% ~ 1.3 % in the 21st century under RCPs, and will be 0.6 %~ 2.2 % in the 2100 - 2299 under RCP 2.6 and 4.5. Under RCP8.5, relative change of annual precipitation is -5.7 % and a wide range of fluctuations is projected with a variance as high as 94.3 in 2100 - 2299, which is 63.2 % higher than the piControl scenario (Fig. 4a-b, Table 5).

The long-term average monthly precipitation shows a single-peak curve, with precipitation highest in July and lowest in December and January. The differences in the long-term average monthly precipitation under RCPs and piControl scenario are projected to grow from -1.9 ~ 1.3 % before 2100 to -5.4 ~ 2.2 % in the period 2100 - 2299 (Fig. 4c-e).

4.2 Calibration and validation of the hydrological models

Previous study found that 1986/1987 was a change-point in the observational period for south China, with more obvious increase of temperature and decrease of precipitation since then (Thomas et al., 2012). Fig. 5 shows that observed annual precipitation and runoff depth in the upper Yangtze River basin in the period 1951 - 1986 are approximately 965 mm and 437 mm, respectively, and decreased by 7 % and 5 % to 895 mm and 415 mm, respectively, in the period 1987 - 2012. Therefore, the period 1979 - 1990, which included both comparatively wet and dry spells, is chosen as the calibration period. Subsequently, hydrological models are validated in two periods without changing the parameters set during the calibration: the wet spell 1967 - 1978, and the dry spell 1991 - 2002.

Based on the NSE, RSR and r values, all four hydrological models perform quite well in both the calibration and validation periods for the simulations of daily discharge at the Cuntan station. In particular, the NSE values of all models exceed 0.75 in the calibration period and 0.7 in the validation periods (Table 6). The KGE values are above the threshold in the calibration period for all models but slightly lower in the validation period for the SWIM and VIC models. The four hydrological models can also properly simulate high flow and low flow represented by Q10 and Q90 in calibration and validation periods. For example, Q10 result illustrates that the several severe floods mentioned previously are reproduced quite well by the model simulations: the peak flows of simulated discharge were 64,300 m^{3}s^{-1}, 53,900 m^{3}s^{-1} and 60,700 m^{3}s^{-1}, respectively, in the 1930s,

1950s and 1990s, deviating by less than 10 % from the recorded peaks (Fig. 6).

To further validate the hydrological models, discharge simulated in another thirty-year historical period (1939 - 1968) is compared with the observed data (Fig. 7). It is found that there are systematic underestimations of streamflow by SWAT, SWIM and VIC. But, all four hydrological models can reproduce the monthly dynamics of river flow quite satisfactorily, with NSE
5   values of 0.79 ~ 0.84 and r values of 0.91 ~ 0.92.

In addition, evapotranspiration outputs of HBV, SWAT, SWIM, VIC are compared with the GLEAM evapotranspiration data (see Section 3.3) in the period 1986 - 2005. The long-term averaged annual evapotranspiration simulated by the four models for the upper Yangtze River basin is 442 mm, 487 mm, 484 mm, 466 mm, respectively, quite close to the result from GLEAM (452 mm). The spatial patterns of the gridded evapotranspiration outputs of the HBV, SWAT, SWIM, VIC model and GLEAM
10   all show low values in the northwest but high values in the southeast of the upper Yangtze River basin (Fig. 8). Furthermore, a matrix consisting of 500 randomly selected pixels from simulated evapotranspiration by VIC and corresponding GLEAM grids is set up to get the kappa value. The deduced kappa value of 0.62 indicates a substantial agreement of two date sources.

4.3 Simulation of daily discharge for 1861 - 2299

The simulated discharge time series for 1861 - 2299 under the piControl scenario without anthropogenic climate change and
15   scenarios with anthropogenic climate change effects are shown in Fig. 9a-b. Similar to precipitation trend, annual mean discharge at the Cuntan station shows no significant trend from 1861 to 2299 under the piControl scenario. In historical period, annual mean discharge has shown a slight decrease trend in 1861 - 2005. Under RCPs, annual mean discharge will be in a significant upward trend by the end of the 21st century with increasing variation in the upper Yangtze River. Annual mean discharge shows no significant change since 2100 under RCP2.6 and RCP4.5, but a rapid decline is projected under high
20   emission RCP8.5 scenario in future (Fig. 9a-b, Table 5).

Comparison of relative changes in mean annual discharge for 2070-2099 and 2270-2299 under RCPs with that of the piControl scenario is presented in Table 7. Relative to the piControl scenario, change of annual mean discharge will be -4.2 %, -1.1 %, -9.1 % and -0.7 % respectively, under RCP2.6, RCP4.5, RCP6.0 and RCP8.5, in 2070 - 2099. And the relative change of annual mean discharge will be 2.2 %, 2.6 % and -30.6 %, respectively, under RCP2.6, RCP4.5 and RCP8.5 in 2270 - 2299 (Table 7).

25   Under RCP2.6 and RCP6.0, Q10 and Q90 discharge will be lower than that under the piControl scenario in 2070 - 2099. The relative changes of Q10 will be 4.3 % higher but that of Q90 will be -3.5 % lower under RCP8.5 than that under the piControl scenario in 2070 - 2099.

In 2270 - 2299, a higher Q10 discharge is projected under RCP2.6 and RCP4.5 than the piControl scenario. Meanwhile, a higher Q90 discharge under RCP2.6 but a lower Q90 discharge under RCP4.5 is projected. But the relative changes of Q10

and Q90 discharge will reach - 13.2 % and - 50.4 % due to the rapid declining of discharge under RCP8.5 in 2270 - 2299. The results indicate there will be more extreme hydrological events in the long run, especially under RCP8.5.

Similar to precipitation and temperature, average monthly discharge in 2070 - 2099 and 2270 - 2299 under both the piControl and RCP scenarios show single peak. Under RCP 4.5, a higher flood volume of August is projected in periods of 2070 -
5   2099 and 2270 - 2299 than the piControl scenario. Meanwhile, a higher volume in 2070 - 2099 but a lower in 2270 - 2299 under RCP8.5 is projected. Under RCP2.6, the flood volume of August is similar to piControl in both periods (Fig. 10a-b). The Generalized Logistic Distribution (GLD), which is the optimistic distribution by Kolmogorov - Smirnov goodness of fit test, is applied to describe the statistical distribution of the daily maximum discharge (represented by annual Q10) for 2070-2099 and 2270-2299. It is found that the return level of daily maximum discharge under RCP2.6, RCP4.5, RCP6.0 and
10   RCP8.5 are higher than piControl scenario in 2070 - 2099 (Fig. 10c). Under RCP 4.5, a higher average of return level of daily maximum discharge is projected in periods of 2070 - 2099 and 2270 - 2299 than the piControl scenario. For RCP8.5, the average of return level of daily maximum discharge is higher in 2070 - 2099 but lower in 2270 - 2299 than piControl scenario. Under RCP2.6, the average of return level of daily maximum discharge is similar to piControl scenario in both periods (Fig. 10c-d).

15   **4.4 Data availability**

The current study generates daily discharge series for the upper Yangtze River at the Cuntan gauging station in the period 1861 - 2299 under scenarios with and without anthropogenic climate change. The river discharge is simulated by four hydrological models, HBV, SWAT, SWIM, and VIC driven by four downscaled and bias-corrected GCMs (GFDL-ESM2M, HadGEM2-ES, IPSL-CM5A-LR and MIROC5), and the datasets are available at https://doi.org/10.4121/uuid:8658b22a-8f98-4043-9f8f-
20   d77684d58cbc (Gao et al., 2019).
(1) Scenario without anthropogenic climate change (piControl):
A total of 16 sequences of daily discharge at the Cuntan hydrological station in the upper Yangtze River are outputs of the four hydrological models that are driven by the four GCMs in the period 1861 - 2299.
(2) Scenarios with anthropogenic climate change:
25   Historical period: A total of 16 sequences of daily discharge at the Cuntan station in the upper Yangtze River are outputs of the four hydrological models that are driven by the four GCMs in the period 1861 - 2005.
RCP2.6 scenario: a total of 16 sequences of daily runoff at the Cuntan station in the upper Yangtze River are outputs of the four hydrological models that are driven by the four GCMs in the period 2006 - 2299 (for GFDL-ESM2M, the sequences are for the period 2006 - 2099).
30   RCP4.5 scenario: a total of 16 sequences of daily discharge at the Cuntan station in the upper Yangtze River are outputs of the four hydrological models that are driven by the four GCMs in the period 2006 - 2099 (for IPSL-CM5A-LR, the sequences are

for the period 2006 - 2299).

RCP6.0 scenario: a total of 16 sequences of daily discharge at the Cuntan station in the upper Yangtze River are outputs of the four hydrological models that are driven by the four GCMs in the period 2006 - 2099.

RCP8.5 scenario: a total of 16 sequences of daily discharge at the Cuntan station in the upper Yangtze River are outputs of the four hydrological models that are driven by the four GCMs in the period 2006 - 2099 (for IPSL-CM5A-LR, the sequences are for the period 2006 - 2299).

5 Summary and conclusions

Using four GCMs (GFDL-ESM2M, HadGEM2-ES, IPSL-CM5A-LR and MIROC5), changes in temperature and precipitation in the upper Yangtze River basin are analysed from 1861 to the end of 23th century under conditions with anthropogenic climate change and for a scenario without anthropogenic climate change (abbreviated as the piControl scenario). The discharge at the Cuntan station in the period 1861 - 2299 is simulated by four hydrological models (HBV, SWAT, SWIM and VIC) driven by the four GCMs, and changes in discharge in a warming world are compared with those under the piControl scenario.

To ensure the reliability of simulated runoff, a multi-objective automatic calibration programme using a univariate search technique is applied to obtain the optimal parameter set for each hydrological model. For the objective functions, the daily discharge and the indicators of high and low flow are considered. Four criteria, including the NSE, KGE, RSR and r, are used to evaluate the parameterization results. To assess the models' ability to satisfactorily simulate discharge under different climate conditions, hydrological models are validated both in dry and wet periods. Besides, evapotranspiration outputs by simulation process are compared with remote-sensing-based evapotranspiration from the GLEAM dataset to further validate performance of the models.

Previous studies have shown that HBV, SWAT and VIC hydrological models could be applied to the Cuntan station in the upper Yangtze River after calibration (Huang et al., 2016;Su et al., 2017; Chen et al., 2017). Our study proves that HBV, SWAT, SWIM and VIC models can satisfactorily simulate precipitation-runoff relation in a changing climate. Moreover, simulated extreme peak values in the 1930s, 1950s and 1990s are also in good agreement with the historical documented records of the catastrophic floods in the Yangtze River.

Although the simulation results are tested by several criteria, there are still uncertainties that could influence the outputs. These uncertainties are associated with the GIS data (e.g., landuse data), selection of the GCMs, the model calibration procedure, and exclusion of water management practices, etc (Gerhard, et al., 2018). First, as no dynamic landuse data are available for the historical period before the 1980s and for the future, a static land use for 1990 is used for simulating river discharge before and after the industrial revolution (historical and RCP scenarios). Second, although the most up-to-date climate scenarios are used in this study, downscaling of GCMs and setting of climate scenarios still contribute a lot to the uncertainties in the

hydrological simulations. Third, hydrological models are parameterized using the automatic calibration programme. The parameterization effect and model applicability are assessed according to the NSE, KGE, and RSR criteria. However, due to equifinality, there could be other parameter sets that may result in a similarly good performance. Combination of parameters and not the choice of individual parameter ultimately influences the result (Cheng et al., 2014). There is a lack of analyses on the effects of different parameter combinations in this study, and the uncertainty related to specific parameters in the models needs to be analysed further. Fourth, since the 1990s, human interferences have escalated in the upper Yangtze River. The construction of dikes and reservoirs alter the timing and volume of peak discharge and base flow. Without consideration of effects of human interferences, but rather focus merely on the natural streamflow is one of the limitations in this study.

The datasets generated in our study are the only available long-term and relatively high-precision discharge sequences for the upper Yangtze River, which include 16 combinations of four hydrological models driven by four GCMs. Simulations by multiple hydrological models and GCMs can provide a range of streamflow variations in future, which is a clue for water resource management strategies. According to our simulation results, the daily simulated discharge will be reduced with the decreasing precipitation in the future. Comparison of long-term simulated daily discharge under RCPs with anthropogenic climate change and under the piControl scenario without human-induced climate change can provide support to understand to which extent human-induced climate change may impact hydrological regime in the upper Yangtze River basin.

Author contribution

Chao Gao, Buda Su, Qianyu Zha, Cai Chen and Gang Luo run the hydrological models. Chao Gao, Buda Su and Tong Jiang analysed results and draft the manuscript. Xiaofan Zeng, Jinlong Huang, Min Xiong and Liping Zhang assisted the data processing. Valentina Krysanova provided guidance for the calibration/validation of the models and the description of results. All authors reviewed the resulting inventory and assisted with paper writing.

Competing interests

The authors declare that they have no conflict of interest.

Acknowledgements

This study was jointly supported by the National Key Research and Development Program of China MOST (2018FY10050001), the National Natural Science Foundation of China (41871024), the High-level Talent Recruitment Program of Ningbo University and the cooperation project between the Natural Science Foundation of China and the Pakistan Science Foundation (41661144027). The authors would like to thank the ISI-MIP project for providing the climate data that was used in this study.

References

Arnold, J. G., Srinivasan, R., Muttiah, R. S., and Williams, J. R.: Large area hydrologic modeling and assessment part I: model development, J Am Water Resour As, 34, 73-89, https://doi:10.1111/j.1752-1688.1998.tb05961.x, 1998.

Bergström, S. and Forsman, A.: Development of a conceptual deterministic rainfall-runoff model, Hydrol. Res., 4, 147-170, https://doi.org/10.2166/nh.1973.0012, 1973.

Braud, I., Roux, H., Anquetin, S., Maubourguet, M. M., Manus, C., Viallet, P., and Dartus, D.: The use of distributed hydrological models for the Gard 2002 flash flood event: analysis of associated hydrological processes, J. Hydrol., 394, 162-181, https://doi.org/10.1016/j.jhydrol.2010.03.033, 2010.

Changjiang Water Resources Commission of the Ministry of Water Resources: The flood and drought disasters in the Yangtze River Basin, China Water & Power Press, Beijing, China, 2002.

Chen, J., Gao, C., Zeng, X. F., Xiong, M., Wang, Y. J., Jing, C., Krysanova, V., Huang, J. L., Zhao, N., and Su, B. D.: Assessing changes of river discharge under global warming of 1.5°C and 2°C in the upper reaches of the Yangtze River Basin: Approach by using multiple- GCMs and hydrological models, Quat. Int., 453, 63-73, https://doi.org/10.1016/j.quaint.2017.01.017, 2017.

Cheng, X. G., Zhang, J., and Gong, H. L.: HSPF hydrologic simulation and parameter uncertainty in a semi-arid and semi-humid area, Acta Scientiae Circumstantiae, 34, 3179-3187, 2014.

Dahl, T. A., Kendall A. D., and Hyndman, D. W.: Impacts of Projected Climate Change on Sediment Yield and Dredging Costs, Hydrol. Process., 32, 1223-1234, https://doi.org/10.1002/hyp.11486, 2018.

Dufresne, J. L., Foujols, M. A., Denvil, S., Caubel, A., Marti, O., Aumont, O., Balkanski, Y., Bekki, S., Bellenger, H., Benshila, R., Bony, S., Bopp, L., Braconnot, P., Brockmann, P., Cadule, P., Cheruy, F., Codron, F., Cozic, A., Cugnet, D., de Noblet, N., Duvel, J. P., Ethe, C., Fairhead, L., Fichefet, T., Flavoni, S., Friedlingstein, P., Grandpeix, J. Y., Guez, L., Guilyardi, E., Hauglustaine, D., Hourdin, F., Idelkadi, A., Ghattas, J., Joussaume, S., Kageyama, M., Krinner, G., Labetoulle, S., Lahellec, A., Lefebvre, M. P., Lefevre, F., Levy, C., Li, Z. X., Lloyd, J., Lott, F., Madec, G., Mancip, M., Marchand, M., Masson, S., Meurdesoif, Y., Mignot, J., Musat, I., Parouty, S., Polcher, J., Rio, C., Schulz, M., Swingedouw, D., Szopa, S., Talandier, C., Terray, P., Viovy, N., and Vuichard, N.: Climate change projections using the IPSL-CM5 Earth System Model: from CMIP3 to CMIP5, Clim. Dyn., 40, 2123-2165, https://doi.org/10.1007/s00382-012-1636-1, 2013.

Frieler, K., Lange, S., Piontek, F., Reyer, C. P. O., Schewe, J., Warszawski, L., Zhao, F., Chini, L., Denvil, S., Emanuel, K., Geiger, T., Halladay, K., Hurtt, G., Mengel, M., Murakami, D., Ostberg, S., Popp, A., Riva, R., Stevanovic, M., Suzuki, T., Volkholz, J., Burke, E., Ciais, P., Ebi, K., Eddy, T. D., Elliott, J., Galbraith, E., Gosling, S. N., Hattermann, F., Hickler, T., Hinkel, J., Hof, C., Huber, V., Jägermeyr, J., Krysanova, V., Marcé, R., Schmied, H. M., Mouratiadou, I., Pierson, D., Tittensor, D. P., Vautard, R., Vliet, M., Biber, M. F., Betts, R. A., Bodirsky, B. L., Deryng, D., Frolking, S., Jones, C. D., Lotze, H. K., Lotze-Campen, H., Sahajpal, R., Thonicke, K., Tian, H. Q., and Yamagata, Y.: Assessing the impacts of

1.5 °C global warming – simulation protocol of the Inter-Sectoral Impact Model Intercomparison Project (ISIMIP2b), Geosci. Model Dev., 10, 4321-4345, https://doi.org/10.5194/gmd-10-4321-2017, 2017.

Gao, C., Su, B.D., Krysanova V., Zha Q.Y., Chen C., Luo G., Zeng X.F., Huang J.L., Xiong M., Zhang L.P, Jiang T.: A 439-year daily discharge dataset (1861-2299) for the upper Yangtze River, China. 4TU. Research Data, https://doi.org/10.4121/uuid:8658b22a-8f98-4043-9f8f-d77684d58cbc, 2019.

Gerhard, K. and Flanner, M. G.: Striking stationarity of large-scale climate model bias patterns under strong climate change, Proc. Natl. Acad. Sci. U. S. A., 115, 9462-9466, https://doi.org/10.1073/pnas.1807912115, 2018.

Gupta, H. V., Kling, H., Yilmaz, K. K., and Martinez, G. F.: Decomposition of the mean squared error and NSE performance criteria: implications for improving hydrological modelling, J. Hydrol., 377, 80-91, https://doi.org/10.1016/j.jhydrol.2009.08.003, 2009.

Hattermann, F. F., Krysanova, V., Gosling, S. N., Dankers, R., Daggupati, P., Donnelly, C., Floerke, M., Huang, S., Motovilov, Y., Buda, S., Yang, T., Mueller, C., Leng, G., Tang, Q., Portmann, F. T., Hagemann, S., Gerten, D., Wada, Y., Masaki, Y., Alemayehu, T., Satoh, Y., and Samaniego, L.: Cross-scale intercomparison of climate change impacts simulated by regional and global hydrological models in eleven large river basins, Clim. Change, 141, 561-576, https://doi.org/10.1007/s10584-016-1829-4, 2017.

Hu, M.S. and Luo, C.Z: The historical flood of China, China Bookstore press, Beijing, China, 1992.

Huang, J. L., Wang, Y. J., Su, B., and Zhai, J. Q.: Future Climate Change and Its Impact on Runoff in the Upper Reaches of the Yangtze River Under RCP4.5 Scenario, Meteorological Monthly, 42, 614-620, https://doi.org/10.7519/j.issn.1000-0526.2016.05.011, 2016.

Jones, C. D., Hughes, J. K., Bellouin, N., Hardiman, S. C., Jones, G. S., Knight, J., Liddicoat, S., O'Connor, F. M., Andres, R. J., Bell, C., Boo, K. O., Bozzo, A., Butchart, N., Cadule, P., Corbin, K. D., Doutriaux-Boucher, M., Friedlingstein, P., Gornall, J., Gray, L., Halloran, P. R., Hurtt, G., Ingram, W. J., Lamarque, J. F., Law, R. M., Meinshausen, M., Osprey, S., Palin, E. J., Chini, L. P., Raddatz, T., Sanderson, M. G., Sellar, A. A., Schurer, A., Valdes, P., Wood, N., Woodward, S., Yoshioka, M., and Zerroukat, M.: The HadGEM2-ES implementation of CMIP5 centennial simulations, Geosci. Model Dev., 4, 543-570, https://doi.org/10.5194/gmd-4-543-2011, 2011.

Jung, I. W., Chang, H., and Moradkhani, H.: Quantifying uncertainty in urban flooding analysis considering hydro-climatic projection and urban development effects, Hydrol. Earth Syst. Sci, 15, 617-633, http://doi.org/10.5194/hess-15-617-2011, 2011.

Krysanova V., Donnelly Ch., Gelfan A., Gerten D., Arheimer B., Hattermann F., and Kundzewicz Z.: How the performance of hydrological models relates to credibility of projections under climate change, Hydrolog SCI J., 63, 696-720, https://doi.org/10.1080/02626667.2018.1446214, 2018.

Krysanova V., Hattermann F., and Wechsung F.: Development of the ecohydrological model SWIM for regional impact studies

and vulnerability assessment, Hydrol. Process, 19, 763-783, https://doi.org/10.1002/hyp.5619, 2005.

Lai, C., Reinders, M. J. T., and Wessels, L.: Random subspace method for multivariate feature selection, Pattern. Recogn. Lett., 27, 1067-1076, https://doi.org/10.1016/j.patrec.2005.12.018, 2006.

Lange, S.: Bias correction of surface downwelling longwave and shortwave radiation for the EWEMBI dataset, Earth. Syst. Dynam., 9, 627-645, https://doi.org/10.5194/esd-2017-81, 2018.

Liang, X., Lettenmaier, D. P., Wood, E. F., and Burges, S. J.: A simple hydrologically based model of land surface water and energy fluxes for general circulation models, J. Geophys. Res.-Atmos., 99, 14415–14428, https://doi.org/10.1029/94JD00483, 1994.

Longfield, S. A., Faulkner, D., Kjeldsen, T. R., Macklin, M. G., Jones, A. F., Foulds, S. A., Brewer, P. A., Griffiths, H. M.: Incorporating sedimentological data in UK flood frequency estimation, J. Flood Risk Manag., e12449, https://doi.org/10.1111/jfr3.12449, 2018.

Luo, C.Z. and Le, J.X: The flood of China, China Bookstore press, Beijing, China, 1996.

Maisa, R., Fabrice, L., Julian, R. V., and Andrew, J. C.: Emergence of robust precipitation changes across crop production areas in the 21st century, Proc. Natl. Acad. Sci. U. S. A., 116, 6673-6678, https://doi.org/10.1073/pnas.1811463116, 2019.

Meaurio, M., Zabaleta, A., Boithias, L., Epelde, A. M., Sauvage, S., Sanchez-Perez, J. M., Srinivasan, R., and Autiguedad, I: Assessing the hydrological response from an ensemble of CMIP5 climate projections in the transition zone of the Atlantic region (Bay of Biscay), J. Hydrol., 548, 46-62, https://doi.org/10.1016/j.jhydrol.2017.02.029, 2017.

Miralles, D. G., Holmes, T. R. H., De, J. R. A. M., Gash, J. H., Meesters, A. G. C. A., and Dolman, A. J.: Global land-surface evaporation estimated from satellite-based observations, Hydrol. Earth Syst. Sci., 15, 453-469, https://doi.org/10.5194/hess-15-453-2011, 2011

Moriasi, D. N., Arnold, J. G., Van Liew, M. W., Bingner, R. L., Harmel, R. D., and Veith, T. L.: Model evaluation guidelines for systematic quantification of accuracy in watershed simulations, T. Asabe, 50, 885-900, https://doi.org/10.13031/2013.23153, 2007.

Nash, J. E., and Sutcliffe, J. V.: River flow forecasting through conceptual models part I — A discussion of principles, J. Hydrol., 10, 282-290, https://doi.org/10.1016/0022-1694(70)90255-6, 1970.

Raman Vinna, L., Wuest, A., Zappa, M., Fink, G., and Bouffard, D.: Tributaries affect the thermal response of lakes to climate change, Hydrol. Earth Syst. Sci., 22, 1-40, https://doi.org/10.5194/hess-22-31-2018, 2018.

Ren, Z. H., Zhao, P., Zhang, Q., Zhang, Z. F., Cao, L. J., Yang, Y. R., Zou, F. L., Zhao, Y. F., Zhao, H. M., Chen, Z.: Quality control procedures for hourly precipitation data from automatic weather stations in China, Meteorological Monthly, 36, 123–132, https://doi.org/10.3788/HPLPB20102207.1462,2010. (in Chinese)

Seneviratne, S. I., Rogelj, J., Seferian, R., Wartenburger, R., Allen, M. R., Cain, M., Millar, R. J., Ebi, K. L., Ellis, N., Hoegh-Guldberg, O., Payne, A. J., Schleussner, C. F., Tschakert, P., Warren, R. F.: The many possible climates from the Paris

Agreement's aim of 1.5 degrees C warming, Nature, 558, 41-49, https://doi.org/10.1038/s41586-018-0181-4, 2018.

Stagl, J. C. and Hattermann, F. F.: Impacts of climate change on riverine ecosystems: Alterations of ecologically relevant flow dynamics in the danube river and its major tributaries, Water, 8, 566, https://doi.org/10.3390/w8120566, 2016.

Su, B., Gemmer, M., and Jiang, T.: Spatial and temporal variation of extreme precipitation over the Yangtze River Basin, Quat. Int., 186, 22-31, https://doi.org/10.1016/J.QUAINT.2007.09.001, 2008.

Su, B., Huang, J. L., Zeng, X. L., Gao, C., and Jiang, T.: Impacts of climate change on streamflow in the upper Yangtze River basin, Clim. Change, 141, 533-546, https://doi.org/10.1007/s10584-016-1852-5, 2017.

Su, B., Zeng X. F., Zhai, J. Q., Wang, Y. J., and Li, X. C.: Projected precipitation and streamflow under SRES and RCP emission scenarios in the Songhuajiang River basin, China, Quat. Int., 380, 95-105, https://doi.org/10.1016/j.quaint.2014.03.049, 2015.

Taylor, K. E., Stouffer R. J., and Meehl G. A.: An Overview of CMIP5 and the Experiment Design, B. Am. Meteorol. Soc., 93, 485-498, https://doi.org/10.1175/BAMS-D-11-00094.1, 2012.

Thomas, F., Marco, G., Liu, L., Su, B.: Change-points in climate extremes in the Zhujiang River Basin, South China, 1961–2007, J. Clim., 110: 783-799, https://doi.org/10.1007/s10584-011-0123-8, 2012.

Wang, G. J., Jiang, T., Blender, R., and Fraedrich, K.: Yangtze 1/f discharge variability and the interacting river–lake system, J. Hydrol., 351, 230-237, https://doi.org/10.1016/j.jhydrol.2007.12.016, 2008.

Watanabe, M., Suzuki, T., O'ishi, R., Komuro, Y., Watanabe, S., Emori, S., Takemura, T., Chikira, M., Ogura, T., Sekiguchi, M., Takata, K., Yamazaki, D., Yokohata, T., Nozawa, T., Hasumi, H., Tatebe, H., and Kimoto, M.: Improved climate simulation by MIROC5: mean states, variability, and climate sensitivity, J. Clim., 23, 6312-6335, https://doi.org/10.1175/2010JCLI3679.1, 2010.
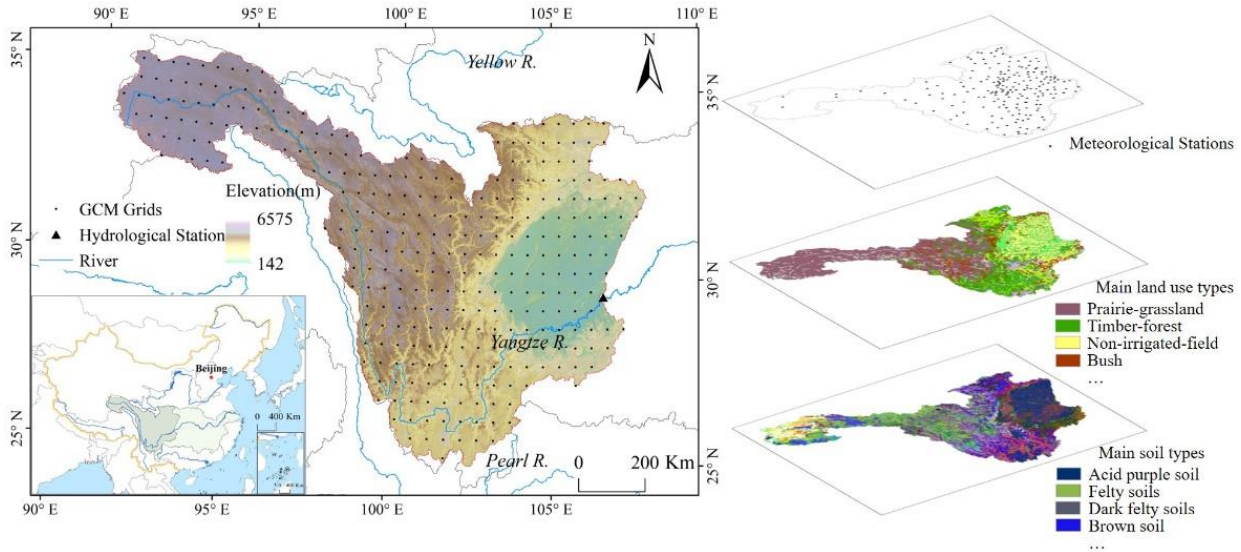
Figure 1 Location of the Cuntan hydrological station, GCM grids, meteorological stations and spatial distribution of the land use and soil types in the upper Yangtze River basin
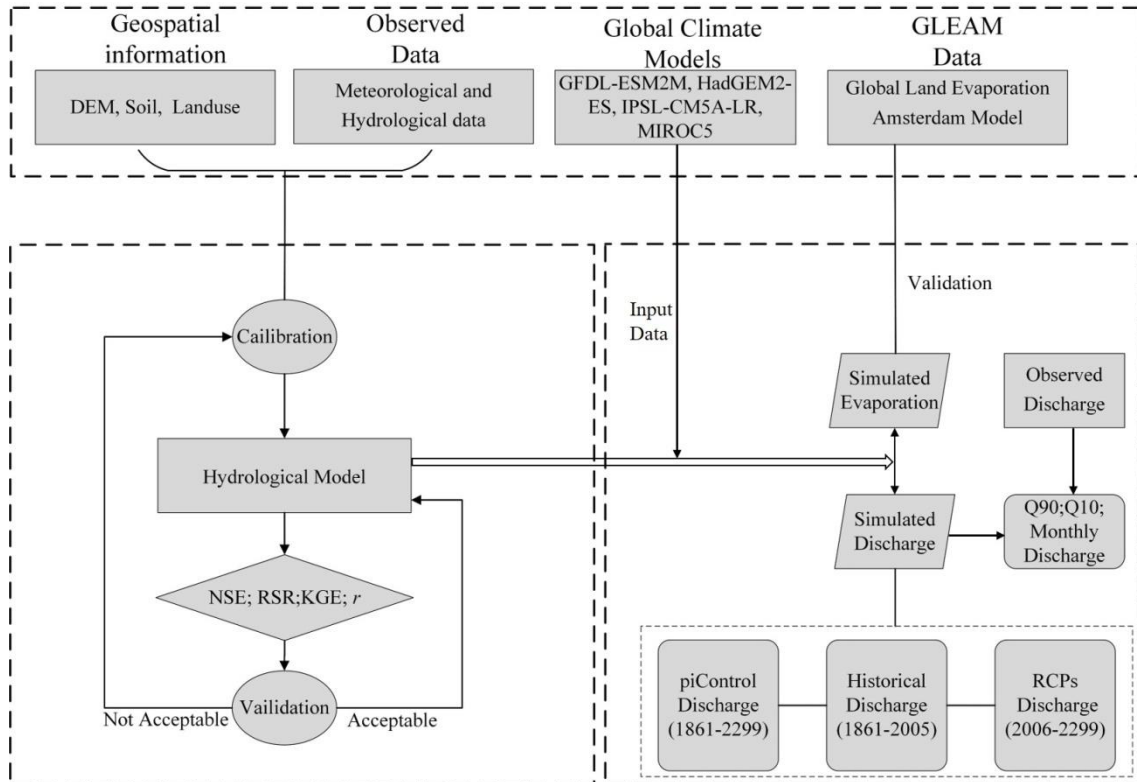
10   **Figure 2 Flowchart for hydrological modelling process**
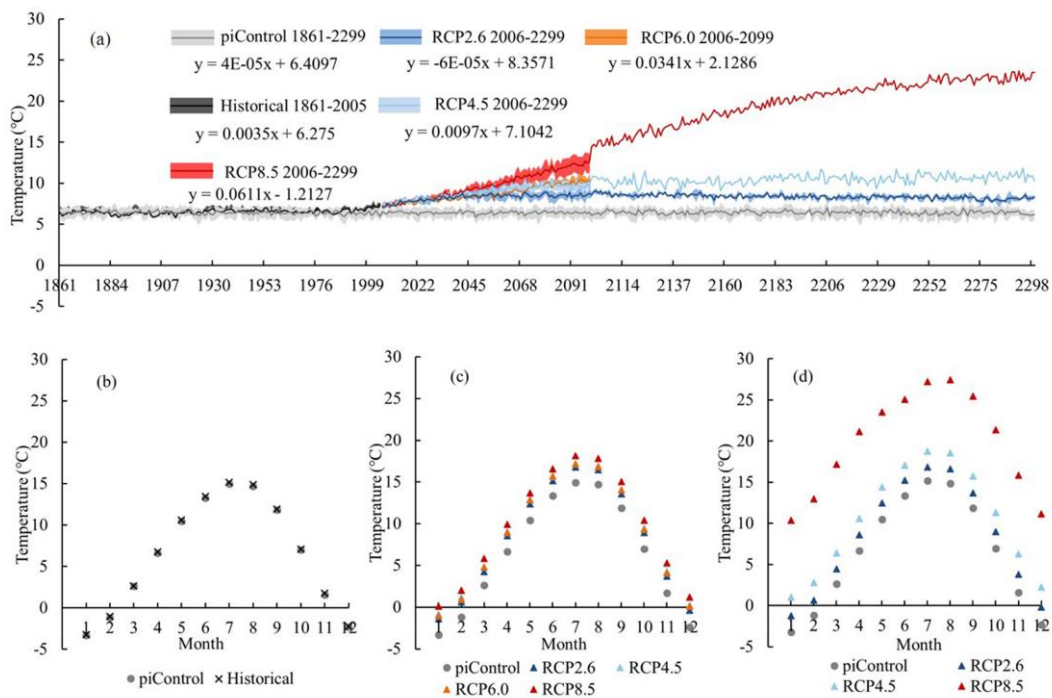
Figure 3 Inter-annual (a) and long-term averaged monthly dynamics (b-d) of the surface air temperature in the upper Yangtze River basin: comparison of the piControl scenario with the anthropogenic climate change scenarios (periods: a: 1861 - 2005; b: 1861 - 2005; c: 2006 - 2099; and d: 2100 - 2299)
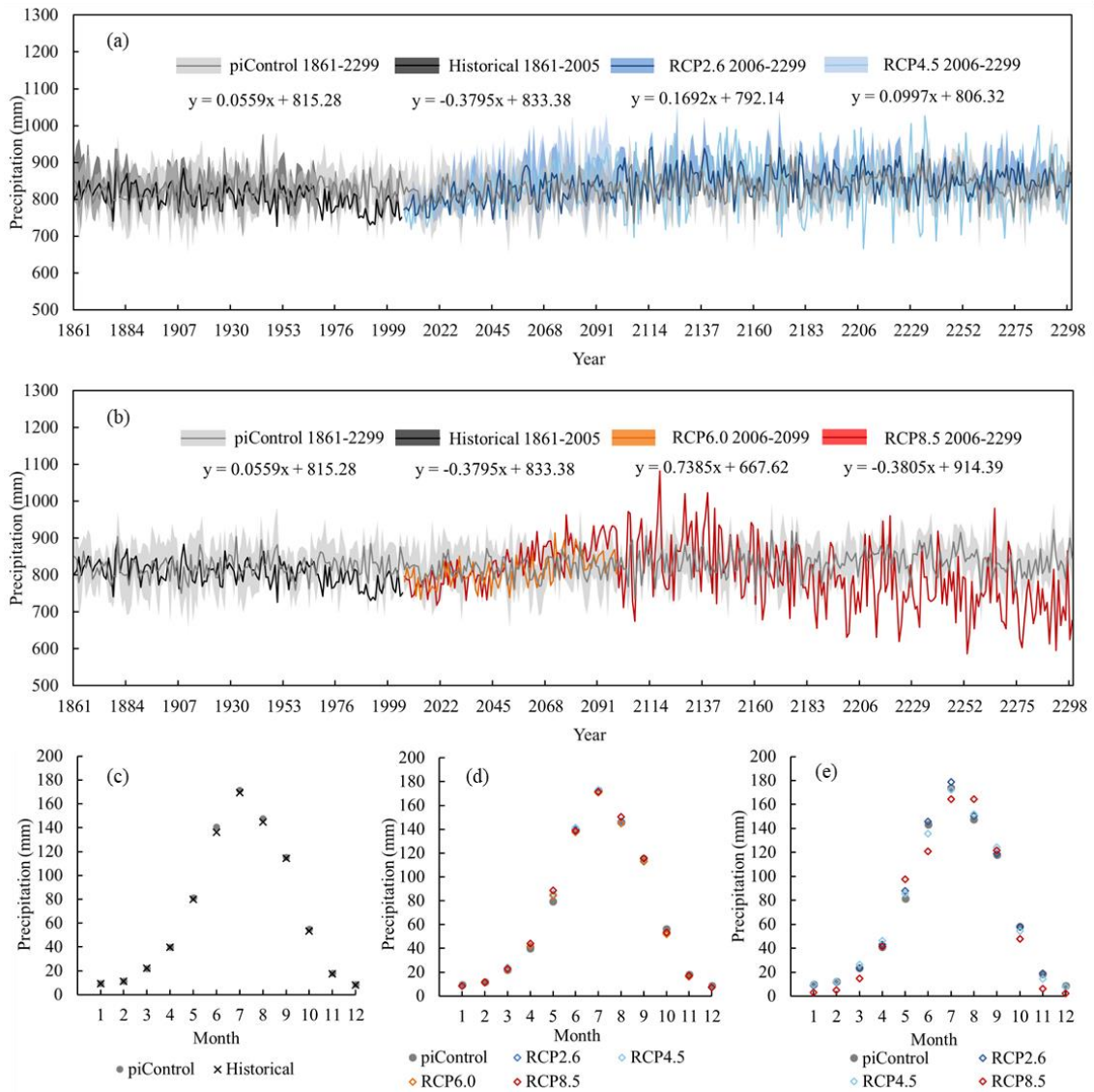
Figure 4 Inter-annual (a-b) and long-term averaged monthly dynamics (c-e) of precipitation in the upper Yangtze River basin: comparison of the piControl scenario with the anthropogenic climate change scenarios (periods: a: 1861-2299; b: 1861-2299; c: 1861 - 2005; d: 2006 - 2099; and e: 2100 - 2299)
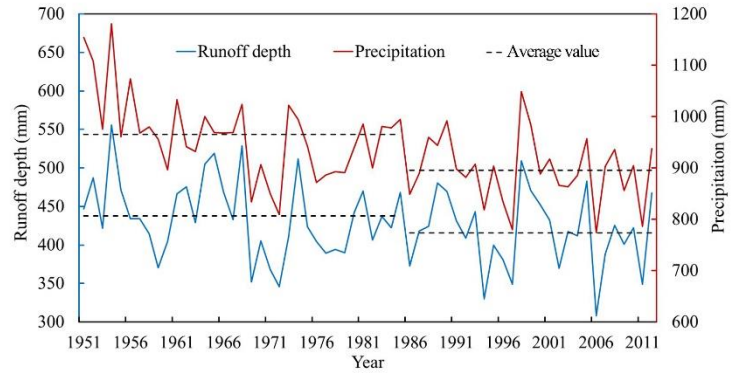
Figure 5 Annual precipitation and runoff depth observed in the upper Yangtze River basin in the period 1951 - 2012
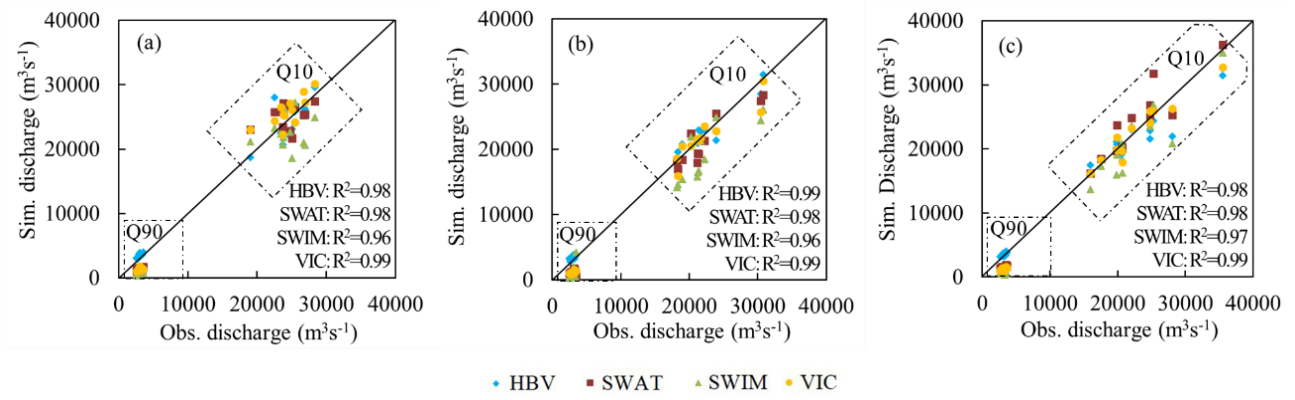
Figure 6 Comparison of the simulated and observed Q10, Q90 percentiles at the Cuntan station in the calibration period 1979 - 1990 (a) and validation period 1967 - 1978 and 1991 - 2002 (b-c)
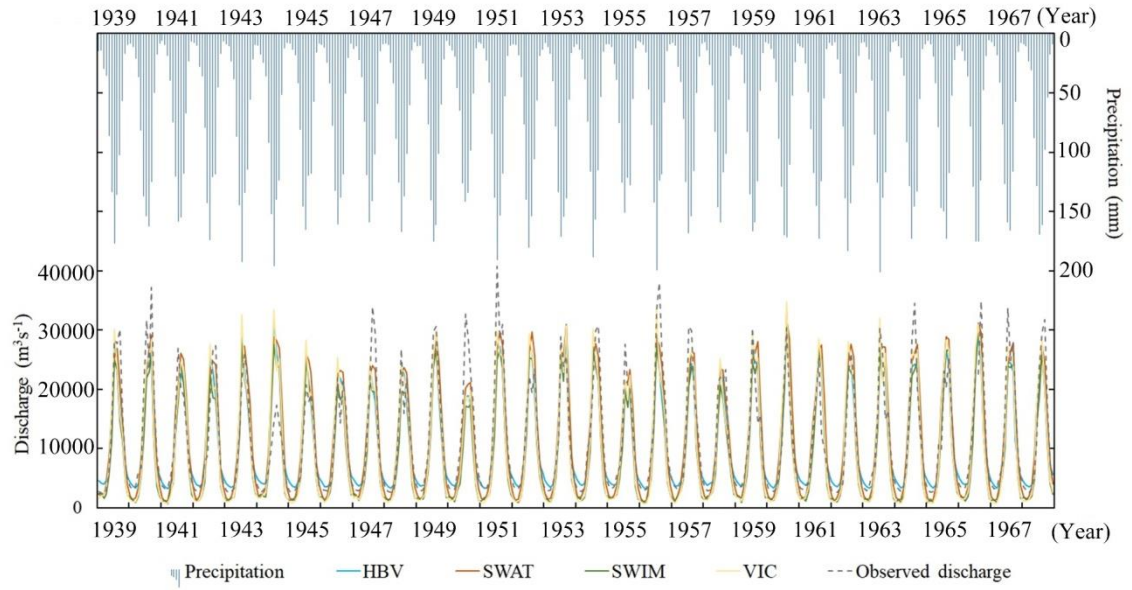
Figure 7 Observed and simulated monthly discharge and precipitation at the Cuntan station in the upper Yangtze basin for 1939 - 1968
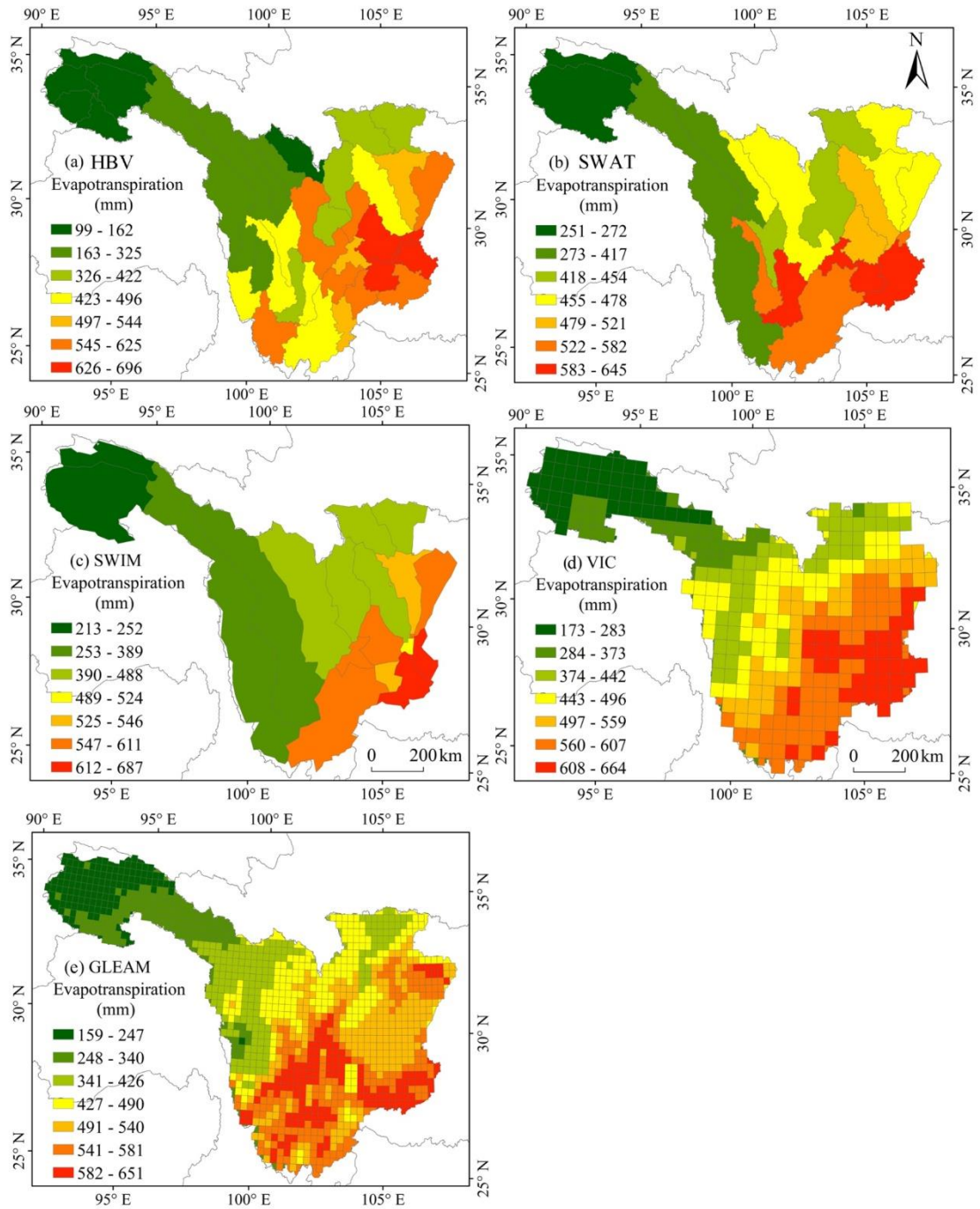
Figure 8 Spatial distribution of multi-year averaged annual evapotranspiration in the upper Yangtze River basin for 1986 - 2005: HBV output (a), SWAT output (b), VIC output (c), SWIM output (d) and GLEAM data(e)
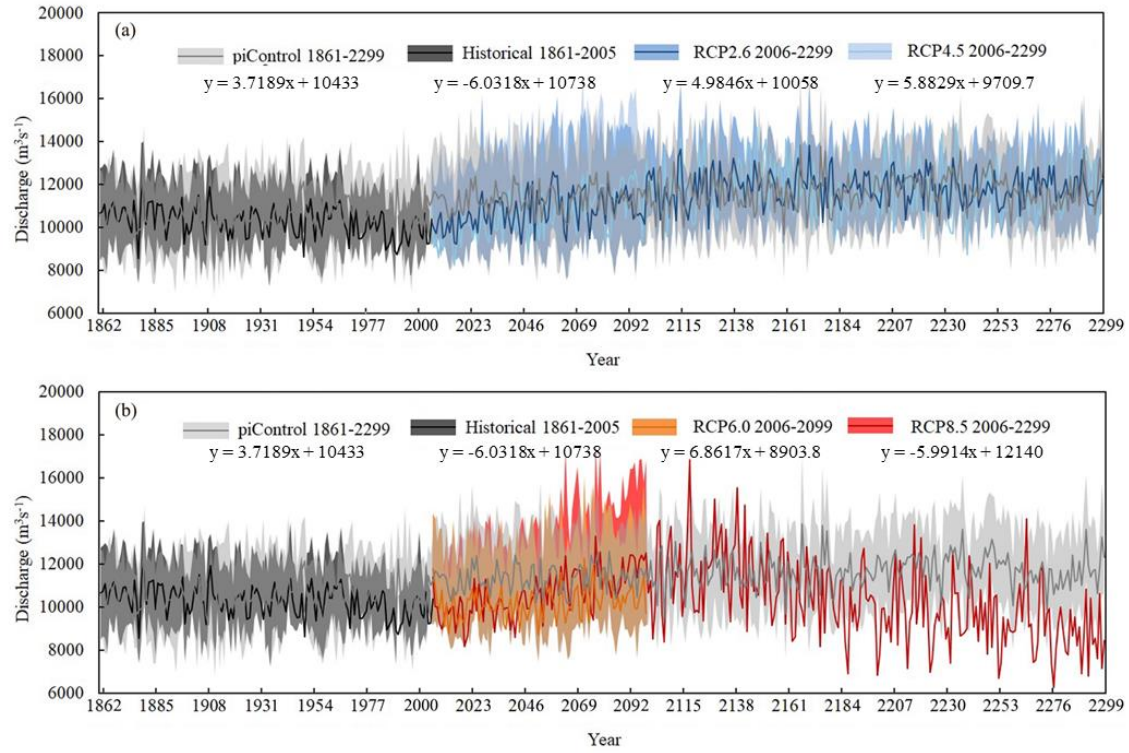
Figure 9 The annual mean discharge at the Cuntan station simulated by four hydrological models (HBV, SWAT, SWIM, and VIC) under the piControl scenario and scenarios with anthropogenic climate change effects (a-b)
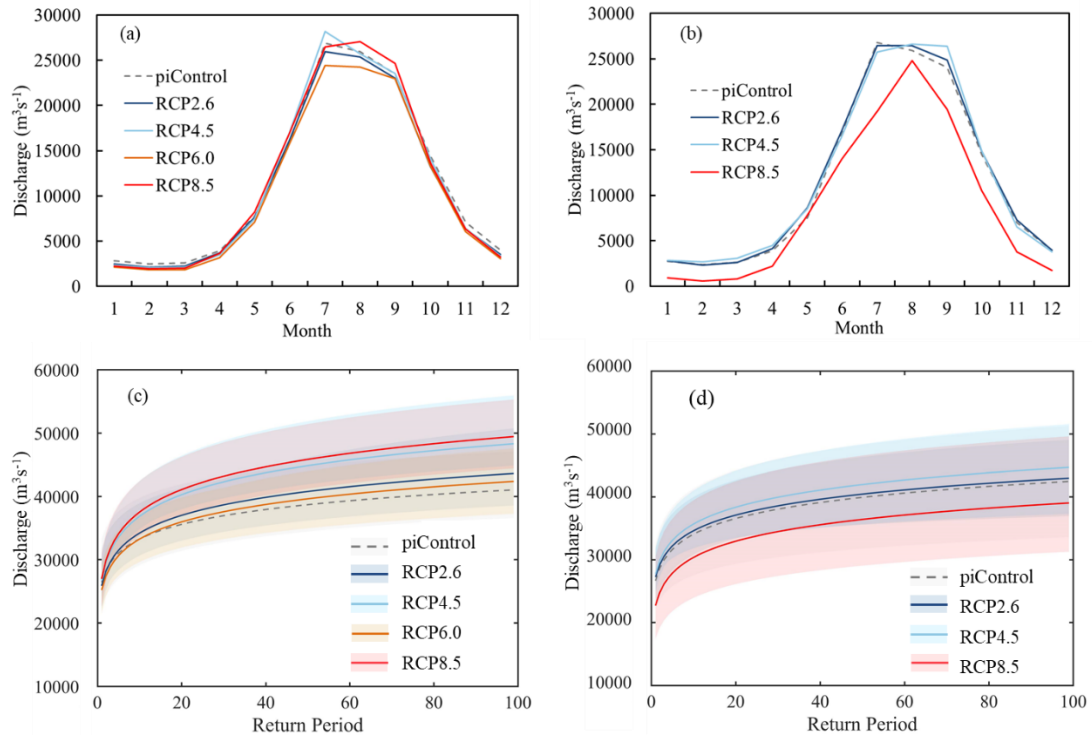
Figure 10 Comparison of monthly mean simulated discharge and return periods of daily maximum discharge at the Cuntan station for 2070 - 2099 (a, c) and 2270 - 2299 (b, d) under RCPs and the piControl scenario

Table 1 Availability of climate scenarios from four GCMs for different periods

Climate scenario	CO_2 concentration	GFDL-ESM2M	HadGEM2-ES	IPSL-CM5A-LR	MIROC5
piControl scenario	286 ppm	1861-2099	1861-2299	1861-2299	1861-2299
Historical scenario	Recorded CO_2	1861-2005	1861-2005	1861-2005	1861-2005
	RCP2.6	2006-2099	2006-2299	2006-2299	2006-2299
Future scenario	RCP4.5	2006-2099	2006-2099	2006-2299	2006-2099
	RCP6.0	2006-2099	2006-2099	2006-2099	2006-2099
	RCP8.5	2006-2099	2006-2099	2006-2299	2006-2099

Table 2 Short description of HBV, SWAT, SWIM, and VIC

Model	Developed Institution	Spatial disaggregation	Representation of soils	Representation of vegetation	Routing method
HBV	Swedish Meteorological and Hydrological Institution	Sub-basins, 10 elevation zones & land use classes	1 soil layer, 2 soil parameters	Fixed monthly plant characteristics	A simple time-lag method
SWAT	United States Department of Agriculture	Sub-basins and hydrological response units	Up to 10 soil layers, 11 soil parameters	A simplified EPIC approach	Muskingum method
SWIM	The Potsdam Institute for Climate Impact Research	Sub-basins and hydrotopes	Up to 10 soil layers, 11 soil parameters	A simplified EPIC approach	Muskingum method, reservoirs and irrigation
VIC	University of Washington, University of California, and Princeton University	Grid of large and uniform cells	3 soil layers, 19 parameters	Fixed monthly plant characteristics	Linearized St. Venant's equations

Table 3 The parameters and their ranges used for calibration of four hydrological models

HBV Name	Range	SWAT Name	Range	SWIM Name	Range	VIC Name	Range
Threshold quick runoff (UZ1)	0-100	Deep aquifer percolation fraction (*Rchrg_Dp*)	0-1	Routing coefficient 1 (*roc1*)	1-100	Non-linear baseflow begins (*Ds*)	0-1
Percolation to lower zone (*PREC*)	0-6	Saturated hydraulic conductivity (*Sol_K*)	0-100	Routing coefficient 2 (*roc2*)	1-100	Maximum baseflow (*Ds_{max}*)	0-30
Non-linearity in soil water zone (*BETA*)	1-5	Maximum canopy storage (*Canmx*)	0-10	Evaporation coefficient (*thc*)	0.5-1.5	Maximum soil moisture (*Ws*)	0-1
Slow time constant upper zone (*KUZ1*)	0.01-1	Average slope steepness (*Slope*)	0-0.6	Baseflow factor for return flow travel time (*bff*)	0.2-1	Variable Infiltration Capacity curve (*b_i*)	0-0.4
Additional precipitation coefficient for snow at gauge (*SKORR*)	1-3	Available water capacity (*Sol_Awc*)	0-1	Coefficient to correct channel width (*chwc0*)	0.1-1	Soil depth 1 (*d_1*)	0.1-1
Precipitation correction for rain (*PKORR*)	0.8-3	Initial SCS CN II value (*Cn2*)	35-98	Saturated conductivity (*sccor*)	0.01-10	Soil depth 2 (*d_2*)	0.1-2
		Groundwater "revap" coefficient (*Gw_Revap*)	0.02-0.2	Groundwater recession rate (*abf*)	0.01-1	Soil depth 3 (*d_3*)	0.1-3
		Biological mixing efficiency (*Biomix*)	0-1	Initial conditions (*gwq0*)	0.01-1		
		Soil evaporation compensation factor (*Esco*)	0-1	Curve number (*cnum*)	10-100		

Table 4 Evaluation criteria for testing simulation capacity of hydrological models

Criterion	Formula	Range	Ideal value	Notation	Reference
Nash-Sutcliffe efficiency (NSE)	$1 - \dfrac{\sum_{t=1}^{N}(Q_{s,t} - Q_{o,t})^2}{\sum_{t=1}^{N}(Q_{o,t} - \bar{Q}_o)^2}$	$(-\infty, 1)$	1	Q_s: simulated discharge; Q_o: observed discharge; $\bar{Q}_o$: mean of observed discharge; $\bar{Q}_s$: mean of simulated discharge; t: sequence of the discharge series; N: number of time steps; α: ratio between the standard deviations of the simulated and observed data; β: ratio between the mean simulated and mean observed discharge	(Nash and Sutcliffe, 1970)
Ratio of the root mean square error and the standard deviation of observation (RSR)	$\dfrac{\sqrt{\sum_{t=1}^{N}(Q_{o,t} - Q_{s,t})^2}}{\sqrt{\sum_{t=1}^{N}(Q_{o,t} - \bar{Q}_o)^2}}$	$(0, +\infty)$	0		(Moriasi et al., 2007)
Pearson's correlation coefficient (r)	$\dfrac{\sum_{t=1}^{N}(Q_{s,t} - \bar{Q}_s)(Q_{o,t} - \bar{Q}_o)}{\sqrt{\sum_{t=1}^{N}(Q_{s,t} - \bar{Q}_s)^2} - \sqrt{\sum_{t=1}^{N}(Q_{o,t} - \bar{Q}_o)^2}}$	$(-1, 1)$	1		(Huang et al., 2012)
Modified Kling -Gupta efficiency (KGE)	$1 - \sqrt{(\alpha - 1)^2 + (\beta - 1)^2 + (r - 1)^2}$	$(-\infty, 1)$	1		(King et al., 2012)

Table 5 Mean values of temperature, precipitation and simulated discharge in different scenarios

		piControl scenario	Historical scenario	Future scenario			
				RCP2.6	RCP4.5	RCP6.0	RCP8.5
Temperature (°C)	1861-2005	6.40	6.53	-	-	-	-
	2006-2099	6.41	-	8.27	8.79	8.70	9.72
	2100-2299	6.43	-	8.38	10.48	-	19.94
Precipitation (mm)	1861-2005	821.8	805.7	-	-	-	-
	2006-2099	819.2	-	814.9	823.8	809.8	830.2
	2100-2299	835.7	-	854.2	841.0	-	790.4
Discharge (m^3s^{-1})	1861-2005	10578.0	10294.4	-	-	-	-
	2006-2099	11338.6	-	10784.6	10592.6	10224.6	10617.8
	2100-2299	11698.5	-	11859.2	11824.3	-	10279.2

Table 6 Performance of four hydrological models in the upper Yangtze River at the calibration period and the wet and dry validation periods

criterion	Thresholds of acceptance	calibration/validation	HBV	SWAT	SWIM	VIC
		1979-1990	0.86	0.81	0.75	0.89
NSE	>=0.7	1967-1978 (wet period)	0.86	0.79	0.7	0.88
		1991-2002 (dry period)	0.86	0.81	0.75	0.89
		1979 - 1990	0.39	0.43	0.50	0.33
RSR	<=0.6	1967-1978 (wet period)	0.38	0.46	0.55	0.34
		1991-2002 (dry period)	0.36	0.42	0.48	0.32
		1979-1990	0.92	0.91	0.91	0.97
r	>=0.9	1967-1978 (wet period)	0.92	0.90	0.89	0.96
		1991-2002 (dry period)	0.94	0.92	0.93	0.97
		1979-1990	0.87	0.9	0.7	0.71
KGE	>=0.7	1967-1978 (wet period)	0.90	0.88	0.65	0.69
		1991-2002 (dry period)	0.85	0.89	0.56	0.68

Table 7 Relative changes in mean annual discharge, Q10 and Q90 in the periods 2070 - 2099 and 2270 - 2299 under the scenarios of anthropogenic climate change relative to the piControl scenario

Period	Scenarios	Relative change of mean discharge (%)	Relative change of Q10 (%)	Relative change of Q90 (%)	Standard deviation	Coefficient of variation
	piControl	-	-	-	607.1	0.05
	RCP2.6	-4.2	-1.2	-5.4	681.1	0.06
2070-2099	RCP4.5	-1.1	3.2	-10.9	997.1	0.09
	RCP6.0	-9.1	-3.5	-10.6	763.7	0.07
	RCP8.5	-0.7	4.3	-3.5	917.3	0.08
	piControl	-	-	-	767.6	0.06
	RCP2.6	2.2	2.5	3.2	608.8	0.05
2270-2299	RCP4.5	2.6	6.6	-2.3	1255.9	0.11
	RCP6.0	-	-	-	-	-
	RCP8.5	-30.6	-13.2	-50.4	1397.4	0.16